Malaysian Journal of Chemistry, 2024, Vol. 26(5), 572-582
(Special Issue: *4th IKMPB Online Symposium 2024 - Development of Chemistry to Accomplish a Sustainable World*)

Synthesis, Characterization, and Liquid Crystalline Behavior of Ester-Schiff Base Derivatives Attached to Nonyl and Tetradecyl Terminal Chains

Nurul Aida Shafinaz Zulaziz[1], Zuhair Jamain[1,2]* and Melati Khairuddean[3]
[1]Organic Synthesis and Advanced Materials (OSAM) Research Group, Faculty of Science and Natural Resources, Universiti Malaysia Sabah, 88400 Kota Kinabalu, Sabah, Malaysia
[2]Green Technologies and Advanced Matter (GreAt) Research Group, Faculty of Science and Natural Resources, Universiti Malaysia Sabah, 88400 Kota Kinabalu, Sabah, Malaysia
[3]School of Chemical Sciences, Universiti Sains Malaysia, 11800 USM, Penang, Malaysia
*Corresponding author (e-mail: zuhairjamain@ums.edu.my)

In this study, a series of ester and Schiff base derivatives, (*E*)-4-((4-n)benzylidene)amino) phenyl-4-nitrobenzoate, was successfully synthesized and characterized. These derivatives consist of nonyl and tetradecyl groups at the end of their chains. The research was done with three reaction schemes: alkylation, condensation, and esterification. All the synthesized compounds were characterized using Fourier transform infrared (FTIR) spectroscopy, nuclear magnetic resonance (NMR) spectroscopy, and CHN elemental analysis. Observation under POM showed that the final compounds with nonyl and tetradecyl terminal chains exhibited a smectic A (SmA) phase in both cycles. These results were further verified by differential scanning calorimetry (DSC) to confirm the mesophase's transition temperature. The structure-property relationship investigations showed the mesogenic compounds to exhibit liquid crystal properties due to the linearity of the molecules, which maintain the rigidity of the core system. In addition, a high number of electronegativity atoms attached resulted in the compound having a high polarizability that induced the liquid crystal behavior.

Keywords: Esterification; Schiff base; liquid crystal; mesogenic; polarizability

Received: January 2024; Accepted: July 2024

Liquid crystalline materials have practical applications in various fields such as display devices, organic light-emitting diodes, anisotropic networks, photoconductors, and semiconductor materials in the realms of science and technology [1–5]. Numerous mesogens, particularly thermotropic liquid crystals, have been created and studied as a result of the high need for new liquid crystals for applications [6, 7]. A liquid crystal (LC) material's molecular architecture, such as a mesogenic core with various connecting groups [8–11], as well as the existence of an alkoxy terminal, has a significant impact on the material's mesophase behavior [12, 13]. Due to their intriguing characteristics, such as their ease of synthesis, chemical stability, and ability to bond stiff core groups, Schiff bases have received a lot of attention [14, 15].

The predominant composition of thermotropic liquid crystals consists of a rigid core comprised of two or more phenyl rings and one or more flexible terminal alkyl chains [16, 17]. The bridging group utilized to connect these rigid core groups is commonly the Schiff base, which is an imine (CH=N). Although it has a stepped core structure, it nonetheless maintains molecular linearity, increasing stability and permitting mesophase development [18, 19]. In addition, enhanced conjugation within the ester moiety introduces some double bond character, resulting in greater stabilization of the mesophase as the conjugation between the substituents and the ester carbonyl (or oxygen) is heightened [20, 21].

Understanding the link between structure and property is crucial to molecular alterations for the creation of new mesogens with desirable properties and potential uses. Alkoxy groups are typical terminal moieties that display liquid crystal characteristics [22]. Strong dipole-moment polar substituents with the capacity to enhance mesomorphic characteristics [23]. The stability of the lattice and melting temperatures are improved by the enhanced dipole moment. The molecules tend to align in a parallel configuration as the length of the terminal substituent grows [24, 25].

This study focused on the synthesis of thermotropic compounds with ester and Schiff base linking units. Jevtovic *et al.* (2023) reported the effect of lateral chloro substituents connected with ester and Schiff base linkages. The findings demonstrated the thermal stability of the sole observed liquid crystal phase, which includes the nematic phase [26]. In order to enhance the strength of mesogenic properties, the synthesized compounds will be adopted with nonyl and tetradecyl terminal chains to induce mesophase

†Paper presented at the 4th IKMPB Online Symposium 2024 – Development of Chemistry to Accomplish a Sustainable World

properties. Extended terminal chains were observed to influence mesophase formation significantly. Compounds with longer alkyl chain lengths typically manifest enantiotropic mesophases, which are thermodynamically stable, while those with shorter alkyl chains display monotropic mesophases, indicating their less stable behavior. Meanwhile, the nitro terminal group's presence increases the compound's polarizability. Hence, new ester-Schiff base derivatives featuring nonyl and tetradecyl terminal chains were synthesized to investigate their molecular interactions and mesophase properties. The ester-Schiff base liquid crystal compounds attached to longer terminal chains are crucial for the operation of liquid crystal displays (LCDs), where electric fields can control the orientation of liquid crystal molecules to modulate high-resolution images.

MATERIALS AND METHODS

Instrumentation

The thin layer chromatography method was employed to monitor the chemical progression of the reaction, while the Perkin Elmer FTIR Microscope Spotlight 200 spectrometer (PerkinElmer) was utilized to ascertain the functional group of the compounds. The chemical structure elucidation was carried out using a Bruker NMR 500 MHz Ultrashield spectrometer (Bruker), and the compounds' purity was confirmed through a CHN analyzer (PerkinElmer). Concurrently, the determination of the mesophase transition was conducted using the POM instrument (Linkam) and further confirmed by the Pyris 1 Differential Scanning Calorimeter (PerkinElmer).

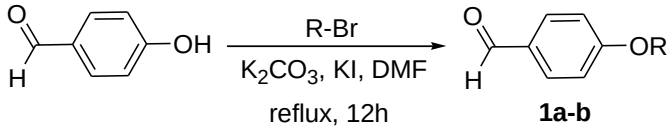

R= C_9H_{19}, **1a**; $C_{14}H_{29}$, **1b**

Scheme 1. Alkylation reaction of intermediates **1a**–**b**.

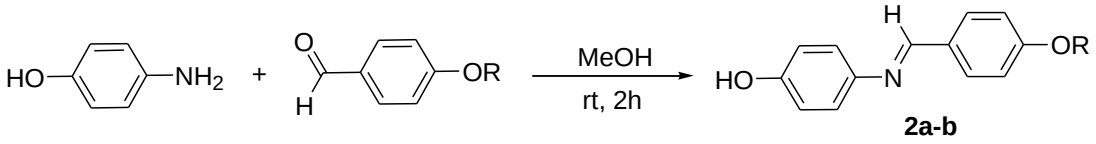

R= C_9H_{19}, **2a**; $C_{14}H_{29}$, **2b**

Scheme 2. Condensation reaction of intermediates **2a**–**b**.

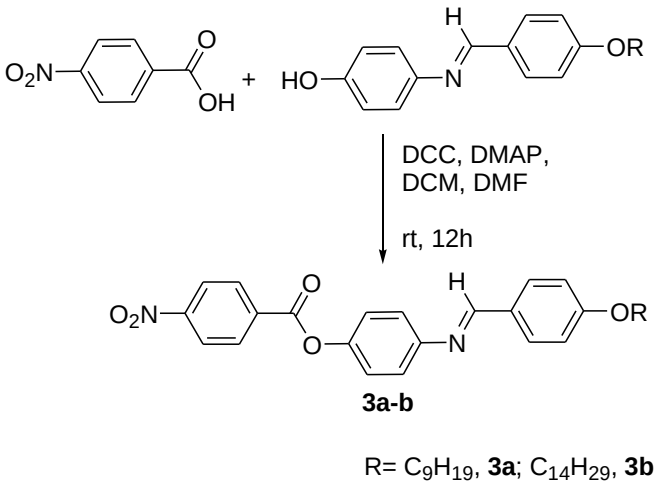

R= C_9H_{19}, **3a**; $C_{14}H_{29}$, **3b**

Scheme 3. Esterification reaction of compounds **3a**–**b**.

Synthesis

The experiment started with the reaction of 4-hydroxybenzaldehyde with alkylated bromide (C_9H_{19} and $C_{14}H_{29}$) to give intermediates **1a**–**b** (Scheme 1) [27, 28]. Then, these intermediates went through a condensation reaction with 4-aminophenol to yield intermediates **2a**–**b** (Scheme 2) [29]. Finally, compounds **3a**–**b** attached to nonyl and tetradecyl terminal chains were produced via esterification reaction (Scheme 3) [30, 31].

Synthesis of 4-(alkyloxy)benzaldehyde, 1a–**b**

4-hydroxybenzaldehyde (0.10 mol) and 1-bromononane (0.10 mol) were separately dissolved in 20 mL of DMF each and both solutions were mixed in a 250 mL round bottom flask. Potassium carbonate, K_2CO_3 (0.15 mol), and potassium iodide, KI (0.01 mol), were added to the mixture. The mixture was refluxed for 12 hours. The reaction's progress was monitored by TLC. Upon completion, the reaction mixture was poured into 250 mL of cold water, and the alkylated compound was extracted with DCM. The organic layers were collected, dried over anhydrous sodium sulfate, and evaporated to form yellowish oil. The same procedure was used to synthesize intermediate **1b**.

4-(nonyloxy)benzaldehyde, 1a

Yield = 6.82 g, (68.07 %), dark yellow oil. FTIR (cm^{-1}): 2913 (C-H sp^3 stretching), 2848 and 2732 (CHO stretching), 1687 (C=O aldehyde), 1598 (aromatic ring C=C stretching), 1247 (C-O stretching). ^{1}H NMR (600 MHz, $CDCl_3$) δ, ppm: 9.79 (s, 1H), 7.73 (d, *J* = 6 Hz, 2H), 6.91 (d, *J* = 6 Hz, 2H), 3.95 (t, *J* = 4.5 Hz, 2H), 1.76-1.70 (m, 2H), 1.42-1.36 (m, 2H), 1.28-1.22 (m, 10H), 0.82 (t, *J* = 3 Hz, 3H). ^{13}C NMR (150 MHz, $CDCl_3$) δ, ppm: 190.56, 164.24, 131.87, 129.77, 114.71, 77.16, 68.37, 31.83, 29.26, 25.93, 22.62, 14.04.

4-(tetradecyloxy)benzaldehyde, 1b.

Yield = 9.69 g, (80.91 %), white powder. FTIR (cm^{-1}): 2913 (C-H sp^3 stretching), 2847 and 2732 (CHO stretching), 1687 (C=O aldehyde), 1598 (aromatic ring C=C stretching), 1249 (C-O stretching). ^{1}H NMR (600 MHz, $CDCl_3$) δ, ppm: 9.85 (s, 1H), 7.81-7.79 (m, 2H), 6.97-6.95 (m, 2H), 4.02 (t, *J* = 8 Hz, 2H), 1.81-1.76 (m, 2H), 1.47-1.41 (m, 2H), 1.36-1.24 (m, 20H), 0.87 (s, 3H). ^{13}C NMR (150 MHz, $CDCl_3$) δ, ppm: 190.76, 164.29, 131.97, 129.79, 114.76, 77.01, 68.45, 31.91, 29.48, 25.95, 22.67, 14.09.

Synthesis of (*E*)-4-((4-(alkyloxy)benzylidene)amino) phenol, 2a–**b**

A mixture of 4-aminophenol (0.01 mol) and intermediate **1a** (0.01 mmol) was dissolved in methanol (40 mL) in a 100-mL round-bottom flask. The reaction mixture was stirred at room temperature for 2 hours. The reaction's progress was monitored by TLC. Upon completion, the mixture was cooled in ice water, and the precipitate formed was filtered and dried. The same procedure was used to synthesize intermediate **2b**.

(*E*)-4-((4-(nonyloxy)benzylidene)amino)phenol, 2a

Yield = 1.77 g, (53.08 %), white powder. FTIR (cm^{-1}): 3165 (O-H stretching), 2918 and 2849 (C-H sp^3 stretching), 1605 (C=N stretching), 1508 (aromatic ring C=C stretching), 1248 (C-O stretching), 1015 (C-N stretching), 841 (C-C stretching). ^{1}H NMR (600 MHz, $CDCl_3$) δ, ppm: 9.41 (s, 1H), 8.49 (s, 1H), 7.81 (d, *J* = 12 Hz, 2H), 7.14 (d, *J* = 12 Hz, 2H), 7.02 (d, *J* = 12 Hz, 2H), 6.78 (d, *J* = 12 Hz, 2H), 4.02 (t, *J* = 9 Hz, 2H), 1.75-1.69 (m, 2H), 1.44-1.38 (m, 2H), 1.33-1.25 (m, 10H), 0.85 (t, *J* = 9 Hz, 3H). ^{13}C NMR (150 MHz, $CDCl_3$) δ, ppm: 161.38, 157.05, 143.47, 130.42, 122.68, 116.12, 68.15, 40.04, 31.74, 29.23, 25.94, 22.55, 14.41.

(*E*)-4-((4-tetradecyloxy)benzylidene)amino)phenol, 2b

Yield = 2.05 g, (51.00 %), white powder. FTIR (cm^{-1}): 3435 (O-H stretching), 2915 and 2848 (C-H sp^3 stretching), 1607 (C=N stretching), 1508 (aromatic ring C=C stretching), 1251 (C-O stretching), 1172 (C-N stretching). ^{1}H NMR (600 MHz, $CDCl_3$) δ, ppm: 8.47 (s, 1H), 7.81 (d, *J* = 6 Hz, 2H), 7.11 (d, *J* = 12 Hz, 2H), 7.02 (d, *J* = 12 Hz, 2H), 6.81 (d, *J* = 12 Hz, 2H), 4.08 (t, *J* = 9 Hz, 2H), 1.79-1.74 (m, 2H), 1.49-1.44 (m, 2H), 1.39-1.29 (m, 20H), 0.88 (d, *J* = 6 Hz, 3H). ^{13}C NMR (150 MHz, $CDCl_3$) δ, ppm: 161.72, 156.82, 144.15, 130.29, 122.31, 116.39, 68.79, 40.7, 31.61, 29.14, 25.88, 22.28, 13.92.

Synthesis of (*E*)-4-((4-(alkyloxy)benzylidene)amino) phenyl-4-nitrobenzoate, 3a-b

A solution of intermediate **2a** (0.05 mol) in DMF (10 mL) was added with 4-nitrobenzoic acid (0.05 mol), dicyclohexylcarbodiimide, DCC (0.05 mol), dimethyl-aminopyridine, DMAP (0.05 mol), and DCM (50 mL) in a 100 mL round-bottom flask. The mixture was stirred at 0 ºC for 1 hour and another 12 hours at room temperature. A cloudy white solid was observed during the stirring process. The reaction's progress was monitored by TLC. Upon completion, the precipitate was filtered, and the filtrate was collected. The filtrate was evaporated to form a precipitate, which was then purified by column chromatography to yield a white powder. The same procedure was used to synthesize compound **3b**.

(*E*)-4-((4-(nonyloxy)benzylidene)amino)phenyl-4-nitrobenzoate, 3a

Yield = 0.44 g, (17.03 %), yellow powder. FTIR (cm^{-1}): 2915 and 2849 (C-H sp^3 stretching), 1738 (ester C=O stretching), 1605 (C=N stretching), 1536 (aromatic ring C=C stretching), 1254 (C-O stretching), 1167 (C-N stretching). ^{1}H NMR (600 MHz, $CDCl_3$) δ, ppm: 8.90 (s, 1H), 8.42-8.37 (m, 4H), 7.86 (d, *J* = 6 Hz, 2H), 7.28

(d, *J* = 6 Hz, 2H), 7.01 (d, *J* = 6 Hz, 2H), 6.75 (d, *J* = 6 Hz, 2H), 4.05 (t, *J* = 6 Hz, 2H), 1.82-1.84 (m, 2H), 1.49-1.47 (m, 2H), 1.38-1.31 (m, 10H), 0.90 (t, *J* = 6 Hz, 3H). ^{13}C NMR (150 MHz, $CDCl_3$) δ, ppm: 190.94, 164.36, 162.16, 160.36, 150.98, 148.26, 144.76, 142.67, 132.07, 131.38, 130.70, 123.82, 122.05, 114.82, 77.10, 68.51, 31.94, 29.33, 26.08, 22.74, 14.19.

(*E*)-4-((4-tetradecyloxy)benzylidene)amino)phenyl-4-nitrobenzoate, 3b

Yield = 0.39 g, (21.59 %), white powder. FTIR (cm^{-1}): 2916 and 2848 (C-H sp^3 stretching), 1739 (ester C=O stretching), 1605 (C=N stretching), 1537 (aromatic ring C=C stretching), 1254 (C-O stretching), 1167 (C-N stretching), 852 (C-C stretching). ^{1}H NMR (600 MHz, $CDCl_3$) δ, ppm: 8.90 (s, 1H), 8.40 (m, 4H), 7.88 (d, *J* = 6 Hz, 2H), 7.29 (d, *J* = 6 Hz, 2H), 7.01 (d, *J* = 6 Hz, 2H), 6.76 (d, *J* = 12 Hz, 2H), 4.08 (t, *J* = 6 Hz, 2H), 1.83-1.81 (m, 2H), 1.48-1.46 (m, 2H), 1.38-1.30 (m, 18H), 0.91 (t, *J* = 6 Hz, 3H). ^{13}C NMR (150 MHz, $CDCl_3$) δ, ppm: 190.94, 164.36, 162.16, 160.36, 150.98, 148.26, 144.76, 142.67, 131.38, 123.82, 122.05, 114.82, 77.10, 68.51, 31.94, 29.24, 26.08, 22.73, 14.19.

RESULTS AND DISCUSSION

FTIR Spectral Discussion

In Figure 1, compound **3a** showcases a functional group encompassing C-H sp^3 stretching, Schiff base, ester, aromatic ring, and ether groups. Specifically, the peaks at 2915 and 2849 $cm^{-1}$are attributed to C-H sp^3 stretching. The symmetrical nature of the molecules contributes to slightly lower frequencies due to the lower intensity and dipole moment of the symmetric mode compared to the asymmetric mode [32].

The impact of linking more than one CH_3 to the carbon is evident in the C-H sp^3 bending region (1465 to 1370 cm^{-1}), resulting in a peak split. Successful alkylation is indicated by the absence of O-H stretching at 3100–3300 cm^{-1}. The relationship between C-H sp^3 stretching and absorption bands at 2915 and 2849 cm^{-1} is notable. Additional absorptions include ester C=O stretching at 1738 cm^{-1}, C=N stretching at 1605 cm^{-1}, and aromatic ring C=C stretching at 1536 cm^{-1}. The presence of C-O stretching is confirmed by a band at 1254 cm^{-1}, while C-N stretching is evident at 1167 cm^{-1}.

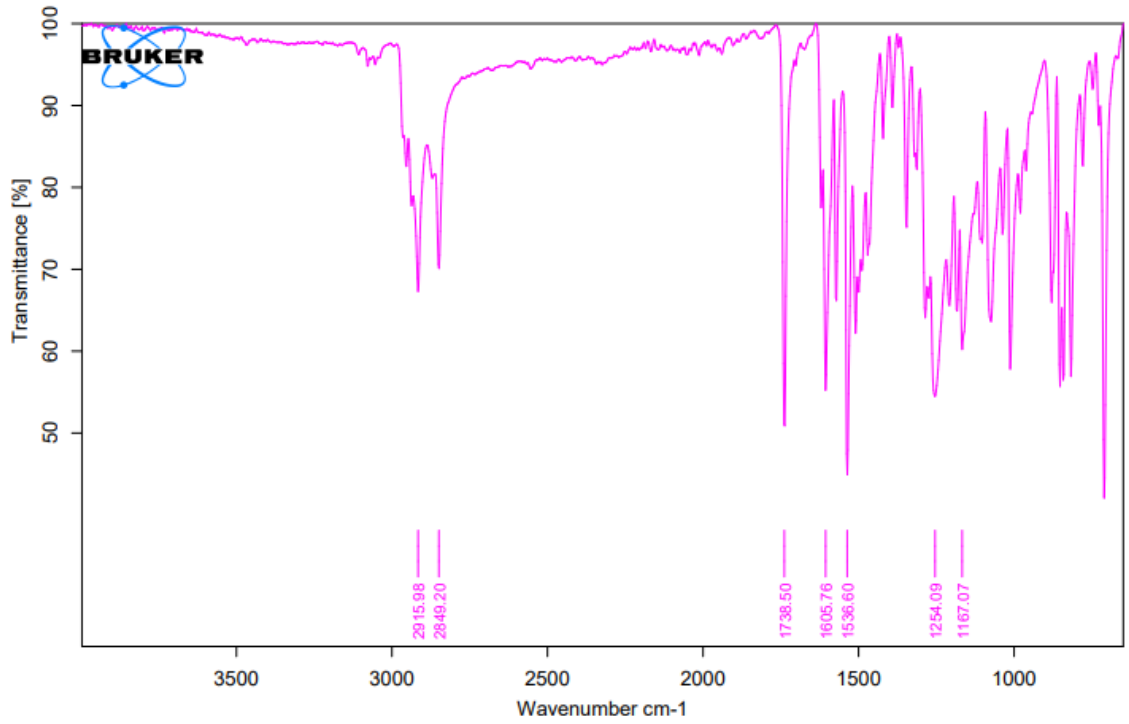

Figure 1. FTIR spectrum of compound **3a**.

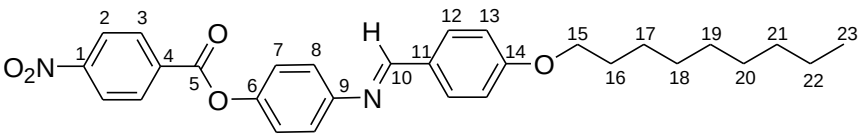

Figure 2. Chemical structure of compound **3a** with complete atomic numbering.

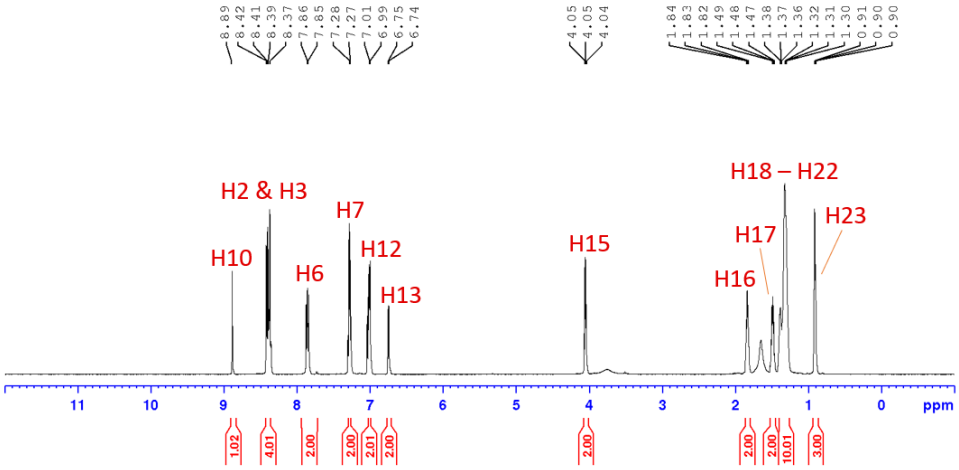

Figure 3. The ^{1}H NMR spectrum (600 MHz, $CDCl_3$) of compound **3a**.

NMR Spectral Discussion

To verify the assigned chemical shifts of the molecules, compound **3a** was selected as a representative. Figure 2 illustrates the structure of compound **3a** with comprehensive atomic numbering, and the ^{1}H NMR spectrum is shown in Figure 3. Complete information on the chemical shift (ppm) and coupling constant (*J*) for compound **3a** is tabulated in Table 1.

In the ^{1}H NMR analysis of both intermediates and compounds, deuterated chloroform was employed as the solvent. The most notable difference in signal between the ^{1}H NMR spectra of the final compounds and those of the intermediates is the absence of signal in the range of δ 9–10 ppm. The absence of this signal shows that the RCHO of the aldehyde group has been fully utilized.

The highest peak, observed at δ 8.89 ppm as a singlet, has been identified as H15, and this occurrence is attributed to the presence of the Schiff base linkage. H2 and H3 exhibit overlapping signals, appearing as a doublet with four hydrogens in the range of δ 8.37 to 8.42 ppm, possibly due to these protons experiencing a similar chemical environment. Other doublets resonate at δ 7.86, 7.28, 7.01, and 6.75 ppm, corresponding to H6, H7, H12, and H13, respectively. A triplet at δ 4.05 ppm is assigned to the ether group (H15), while strong peaks in the range of δ 1.30–1.84 ppm confirm the presence of alkyl chains (H16–H22). Additionally, H23 is situated at δ 0.901 ppm in the most upfield region, representing the methyl group of the alkyl chain.

Figure 4 illustrates the ^{13}C NMR spectrum of compound **3a**. The highest peak in the spectrum, corresponding to C5, is observed at δ 164.29 ppm, attributable to the presence of a C=O linking unit. The peak representing C14 resonates at δ 162.10 ppm, signifying the carbon attached to the O-R group. The peak for C10 is at δ 160.30 ppm, indicating the C=N linking group. Furthermore, the peak for C1 is found at δ 150.92 ppm, denoting the carbon in the benzene ring attached to a nitro group. The peak for C6 is at δ 148.20 ppm, indicating the carbon in the benzene ring attached to a highly electronegative oxygen atom O. Subsequently, a peak at δ 144.70 ppm indicates C9 is connected to an electronegative nitrogen atom, which is lower than the oxygen atom. The other quaternary carbons, C4 and C11, resonated at δ 142.61 and 132.01 ppm, respectively. The methine carbons (C-H) of the *p*-aromatic rings resonated at δ131.32, 130.64, 123.76, 121.99, and 114.76 ppm, which were assigned to C2, C3, C7, C8, C12, and C13, respectively. The linkage of the alkyl chain to the ether group at C15 is confirmed by a peak at δ 68.45 ppm. Within the alkyl chain, C16 to C22 exhibit peaks ranging from δ 22.68 to 31.87 ppm. The most upfield signal, denoting the presence of C23, representing the methyl group, is detected at δ 14.13 ppm.

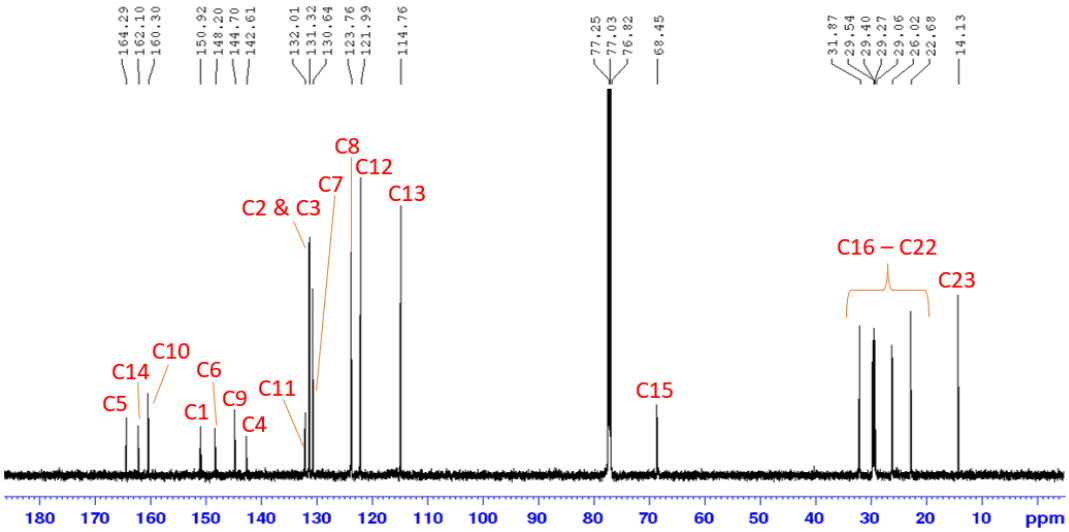

Figure 4. The ^{13}C NMR spectrum (150 MHz, $CDCl_3$) of compound **3a**.

Table 1. Summarized NMR spectral data of compound **3a**.

Proton	^{1}H-NMR [δ (ppm), multiplicity, coupling constant (Hz)]	Carbon	^{13}C-NMR [δ (ppm)]
H10	8.89 (s)	**C10**	160.30
H2	6.54 (d, *J* =12.0 Hz)	**C2**	131.32
H3		**C3**	
H7	6.54 (d, *J* = 6.0 Hz)	**C7**	130.64
H8	6.54 (d, *J* = 6.0 Hz)	**C8**	123.76
H12	6.54 (d, *J* =12.0 Hz)	**C12**	121.99
H13	6.54 (d, *J* = 6.0 Hz)	**C13**	114.76
H15	4.05 (t, *J* = 6.0 Hz)	**C15**	68.45
H16-H22	1.30-1.84 9 (m)	**C15-C22**	22.68-31.87
H23	0.90 (t, *J* = 6.0 Hz)	**C23**	14.13

Table 2. Phase sequence for compounds **3a** and **3b**.

Compound	Mode	Transition temperature (°C)				
3a	**Heating**	**Cr**		**SmA**		**I**
		•	177.60	•	210.03	•
	Cooling	**I**		**SmA**		**I**
		•	209.18	•	173.67	•
3b	**Heating**	**Cr**		**SmA**		**I**
		•	190.45	•	234.55	•
	Cooling	**I**		**SmA**		**I**
		•	230.80	•	187.50	•

Note: **Cr** = Crystal, **SmA** = Smectic A, **I** = Isotropic

Determination of Liquid Crystal Property using POM

In Table 2, it is observed that compounds **3a**–**b** display liquid crystal behavior consistently during both heating and cooling cycles, manifesting phases described as liquid crystalline. Compound **3b** exhibits a notably higher melting point than compound **3a**. This difference is ascribed to an increase in the van der Waals forces in compound **3b** compared to compound **3a**. The longer chain length at the terminal chain in **3b** requires more energy to break this bond, ultimately resulting in the observed higher melting point [33].

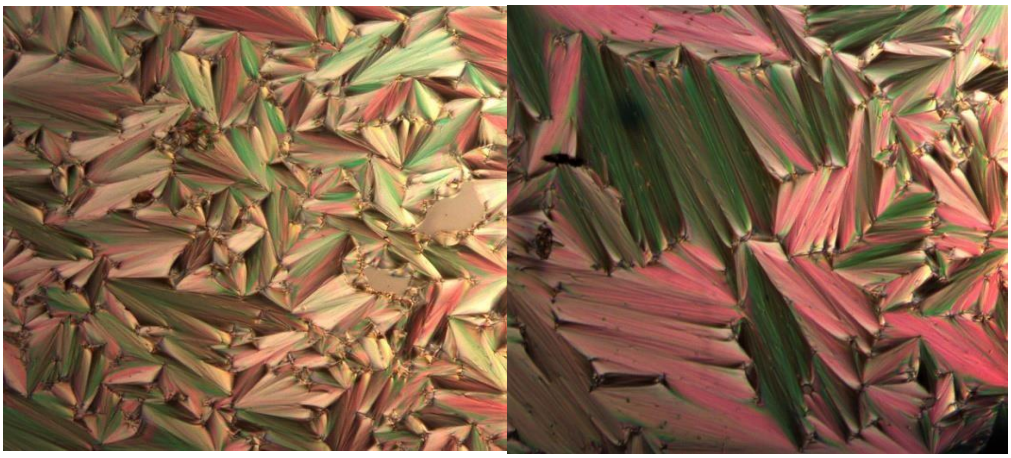

(a) (b)

Figure 5. The POM photomicrographs of cooling cycle showing the SmA phase for (a) compound **3a** at 187.55 ºC, and (b) compound **3b** at 192.31 ºC (Magnification of 20 × 0.50).

During the heating phase, compound **3a** exhibited a smectic A phase at 177.60 ºC and became isotropic at 210.03 ºC. Upon cooling, the SmA was formed at 209.18 ºC before forming a crystal texture at 173.67 ºC. Meanwhile, compound **3b** showed the same trend of Cr-SmA-I in both cycles. The textures of compounds **3a** and **3b** are illustrated in Figure 5.

Determination of Liquid Crystal Property using DSC

Compound **3a** was chosen as a representative for the comprehensive discussion of DSC results since compound **3b** exhibits similar trends. Figure 6 presents the data obtained for the formation of phases during the heating and cooling cycles.

During the heating cycle, two peaks were observed at 177.60 ºC (3.5 kJ/mol), indicating the transformation of the crystal into the smectic A phase, demonstrating its liquid crystal nature. The process of heating was continued to 210.03 ºC (6.28 kJ/mol), which makes it in isotropic phase as a liquid form. The emergence of all these peaks demonstrated the use of endothermic energy absorbed by the crystal molecules to dismantle the intermolecular interactions between molecules [34].

In the cooling cycle, only two peaks were observed, offering valuable insights into the phases of transformation that occurred. The cooling cycle began at 209.18 ºC (-7.10 kJ/mol^{-1}), indicating that the liquid has already undergone the process of cooling into the smectic A phase from the isotropic phase. The cooling process continued until 173.67 ºC (-4.26 kJ/mol^{-1}) to reach the solid crystal phase. The development of these peaks demonstrated that the exothermic energy absorbed by the liquid crystal molecules was utilized to create intermolecular interactions between molecules. Enthalpy measurements showed that this transition is different from solid to liquid crystal in that less latent heat is required for the latter [35].

Structure Properties Relationship

POM was used to monitor and observe the properties of liquid crystals that were displayed by compounds **3a** and **3b**. Important aspects of liquid crystal qualities include the chain length of a compound's terminal group, the presence of a suitable core, and the existence of connecting units [36, 37]. In this specific scenario, the longer alkyl chain of the compounds made the molecule more flexible, thereby promoting mesophase behavior within the compound [38]. As the alkyl chain lengthens, the compound's melting point also rises [39]. Consequently, a higher melting point enhances the polarizability of compounds within the same series. Therefore, the propensity to exhibit the property of the smectic layer has increased as a result of the enhancement of the cohesive forces between the sides (the terminal group) and the core of the molecules [40]. Molecules that display smectic phase behavior are more likely to favor lamellar packing than other types of molecular packing due to an increase in the number of van de Waals connections and the likelihood of interweaving between the alkoxy chains [41, 42].

In this study, compounds **3a** and **3b** with terminal alkoxy chains of nonyl and tetradecyl exhibited liquid crystal behavior because of the powerful attractive forces that they have. As the length of the alkyl chain increases, there is an increased likelihood that the smectic phase will be present in this context. This is because of the inherent flexibility of the long chains, which has the effect of increasing the clearing temperature [43]. This tendency is observable in compounds **3a** and **3b**, which only displayed the smectic phase in their crystalline structures.

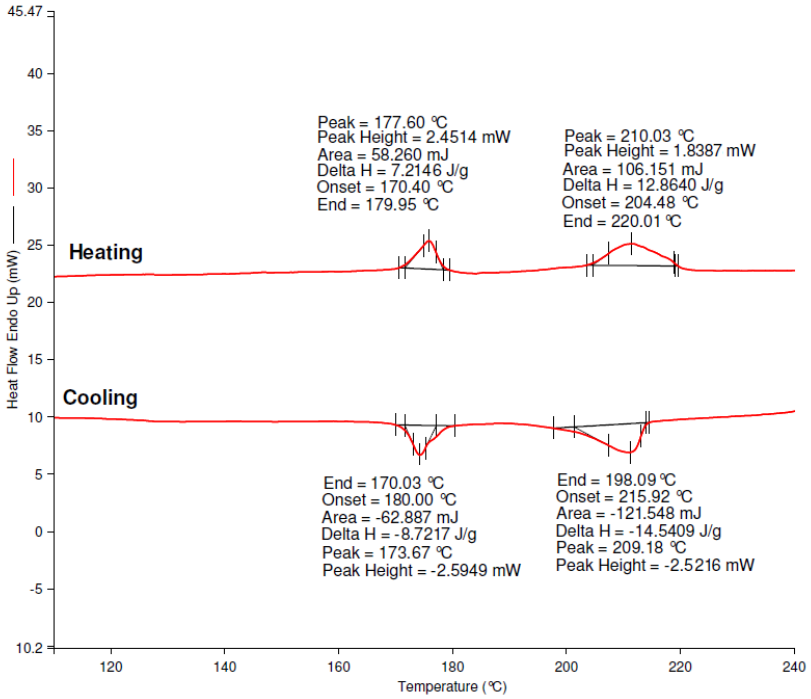

Figure 6. DSC thermogram of compound **3a**

The smectic phase is the most organized of the different phases, having a higher degree of organization than the others. As a consequence of this, good molecular packing is necessary for the creation of stable phases [44, 45].

Moreover, the impact of the Schiff base (–C=N–) linking unit was also investigated. Upon conjugation with the phenylene rings, the molecules experienced an increase in length, leading to enhanced anisotropic polarizability and flexibility [46]. Consequently, the rigidity and linearity of the constituents were preserved, contributing to diverse property modifications in mesomorphic materials [47]. The incorporation of ester linkage in the molecule has led to some double bonding, whereby the mesophase is more stabilized [48]. Hence, the presence of ester-Schiff base linkages caused compounds **3a** and **3b** to adopt mesomorphic properties.

CONCLUSION

A new series of ester and Schiff base derivatives with nonyl and tetradecyl terminal chains has been successfully synthesized and characterized. The structure elucidation of all compounds aligns well with data from Fourier transform infrared (FTIR) spectroscopy, nuclear magnetic resonance (NMR) spectroscopy, and CHN elemental analysis. Polarized optical microscopy (POM) was applied in order to analyze the liquid crystal characteristics of compounds **3a**–**b** and further confirm the transition using differential scanning calorimetry (DSC). These compounds were found to exhibit smectic A liquid crystal characteristics due to their linear structure and electronegative atoms, which resulted in high polarizability.

ACKNOWLEDGEMENT

The authors would like to acknowledge the funding from the Universiti Malaysia Sabah, Grant Number DKP0041 and SPB0004-2020.

The authors declare that they have no conflict of interest.

REFERENCE

1. Ma, J., Xuan, L. (2013) Towards nanoscale molecular switch-based liquid crystal displays. *Displays*, **34**, 293–300.

2. Iqbal, D., Samiullah, M. S. (2013) Photo-responsive shape-memory and shape-changing liquid-crystal polymer networks. *Materials*, **6**, 116–142.

3. Missaoui, T., Ben Amor, I., Soltani, T., Ben Ouada, H., Jeanneau, E., Chevalier, Y. (2020) Dielectric and electro-optic properties of cybotactic nematic phase in hydrogen-bonded liquid crystals. *Journal of Molecular Liquids*, **304**, 112726.

4. Balakrishnan, V., Phan, H. P., Dinh, T., Dao, D. V., Nguyen, N. T. (2017) Thermal flow sensors for harsh environments. *Sensors*, **17**, 2061

5. Popov, P., Honaker, L., Kooijman, E. E., Mann, E. K., Jákli, A. (2016) A liquid crystal biosensor for specific detection of antigens. *Sensing and Bio-Sensing Research*, **8**, 31–35.

6. Carlescu, I. (2018) Introductory Chapter: Liquid Crystals. In *Liquid Crystals—Self-Organized Soft Functional Materials for Advanced Applications*; *IntechOpen: Bucharest, Romania*.

7. Xi, X., Yan, C., Shen, L. Z., Wang, Y., Cheng, P. (2023) Liquid crystal photoalignment technique: Basics, developments, and flexible/stretchable device applications. *Materials Today Electronics*, **6**, 100069.

8. Thaker, B. T., Patel, P. H., Vansadiya, A. D., Kanojiya, J. B. (2009) Substitution effects on the liquid crystalline properties of thermotropic liquid crystals containing Schiff base chalcone linkages. *Molecular Crystals and Liquid Crystals*, **515**, 135–147.

9. Jamain, Z., Omar, N. F., Khairuddean, M. (2020) Synthesis and determination of thermotropic liquid crystalline behavior of cinnamaldehyde-based molecules with two Schiff base linking units. *Molecules*, **25**, 3780.

10. Nafee, S. S., Hagar, M., Ahmed, H. A., Alhaddad, O., El-Shishtawy, R. M., Raffah, B. M. (2020) New two rings Schiff base liquid crystals; ball mill synthesis, mesomorphic, Hammett and DFT studies. *Journal of Molecular Liquids*, **299**, 112161.

11. Ahmed, N. H. S., Saad, G. R., Ahmed, H. A., Hagar, M. (2020) New wide-stability four-ring azo/ester/Schiff base liquid crystals: synthesis, mesomorphic, photophysical, and DFT approaches. *RSC Advances*, **10**, 9643–9656.

12. Nawawi, M. F., Salleh, N. M., Lee, V. S., Cheng, S. -F. (2023) Synthesis, characterization and structure-mesomorphic properties relationship of palm-based azo-ester bridged liquid crystals from caprylic acid. *Industrial Crops and Products*, **199**, 116765.

13. Jamain, Z., Khairuddean, M., Loh, M. L., Manaff, N. L. A., Makmud, M. Z. H. (2020) Synthesis and characterization of hexasubstituted cyclotriphosphazene derivatives with azo linking units. *Malaysian Journal of Chemistry*, **22**, 125–140.

14. Sun, J. -T, Ge, Z. -X., Li, C. -Y., Zhang, Z. -Y., Wang, Y. -M., Jia, Y. -G., Tian, M., Yao, D. -S. (2023) Novel branched liquid crystal oligomers containing azo and Schiff base groups. *Journal of Molecular Structure*, **1273**, 134322.

15. Lee, W. N., Salleh, N. M., Velayutham, T. S., Cheng, S. -F. (2023) Synthesis, phase transition behavior and dielectric properties of smectogenic palm-based liquid crystals containing Schiff base ester and phenyl ring. *Journal of Molecular Structure*, **1282**, 135168.

16. Wang, Q., Chen, H., Xing, H., Deng, Y., Luo, Z. -W., Xie, H. -L. (2021) Long rod-like liquid crystal containing azobenzene and the applications in phase-transition regulation and orientation of nematic liquid crystal. *Crystals*, **11**, 418.

17. Jamain, Z., Habil, S., Makmud, M. Z. H., Khairuddean, M. (2021) Synthesis, structural and dielectric characteristics of liquid crystalline azo-based compounds with different terminal length. *In Proceedings of the 2021 IEEE International Conference on the Properties and Applications of Dielectric Materials (ICPADM), Johor Bahru, Malaysia, 12–14 July 2021*, 49–52.

18. Jamain, Z., Azman, A. N. A., Razali, N. A., Makmud, M. Z. H. (2022) A review on mesophase and physical properties of cyclotriphosphazene derivatives with Schiff base linkage. *Crystals*, **12**, 1174.

19. Al-Mutabagani, L. A., Alshabanah, L. A., Ahmed, H. A., Alalawy, H. H., Al Alwani, M. H. (2021) Synthesis, mesomorphic and computational characterizations of nematogenic Schiff base derivatives in pure and mixed state. *Molecules*, **26**, 2038.

20. Soni, R., Nakum, K. J., Katariya, K. D., Soman, S. S., Nada, N., Hagar, M. (2023) Synthesis, mesomorphic properties and DFT calculations of new coumarin Schiff base-ester liquid crystals. *Liquid Crystals*, **50**, 636–651.

21. Selvarasu, C., Kannan, P., (2016) Effect of azo and ester linkages on rod shaped Schiff base liquid crystals and their photophysical investigations. *Journal of Molecular Structure*, **1125**, 234–240.

22. Jamain, Z., Khairuddean, M., Kamaruddin, K., Rui, Y. (2021) Synthesis, structural elucidation and mesophase behavior of hexasubstituted cyclotriphosphazene molecules with amide linking unit. *Malaysian Journal of Chemistry*, **23**, 213–225.

23. Avani, R. R., Bhoya, U. C. (2019) Mesomorphism dependence on molecular rigidity and flexibility. *Molecular Crystals and Liquid Crystals*, **665**, 43–51.

24. Alnoman, R., Al-Nazawi, F. K., Ahmed, H. A., Hagar, M. (2019) Synthesis, optical, and geometrical approaches of new natural fatty

acids' esters/Schiff base liquid crystals. *Molecules*, **24**, 4293.

25. Uhood, J. A., Tarik, E. G., Howraa, H. R. (2010) Synthesis and characterization of azo compounds and study of the effect of substituent on their liquid crystalline behavior. *Molecules*, **15**, 5620–5628.

26. Jevtovic, V., Ahmed, H. A., Khan, M. T., Al-Zahrani, S. A., Masood, N., Jeilani, Y. A. (2023) Preparation of laterally chloro-substituted Schiff base ester liquid crystals: mesomorphic and optical properties. *Crystals*, **13**, 835.

27. Amiruddin, N. S., Jamain, Z., Khairuddean, M. (2023) Synthesis, characterization and liquid crystalline behavior of 4-((e)-(((e)-4-(decyloxy) benzylidene)hydrazineylidene) methyl)phenol. *Malaysian Journal of Chemistry*, **25**, 517–524.

28. Jeong, M. J., Park, J. H., Lee, C., Chang, J. Y. (2006) Discotic Liquid Crystalline Hydrazone Compounds: Synthesis and Mesomorphic Properties. *Organic Letters*, **8**, 2221–2224.

29. Jamain, Z., Khairuddean, M. (2021) Synthesis and Mesophase behavior of benzylidene-based molecules containing two azomethine units. *Proceedings of the Journal of Physics: Conference Series; IOP Publishing Ltd.*, **1882**, 012120.

30. Katariya, K. D., Nakum, K. J., Soni, H., Nada, S., Mohamed Hagar, M. (2023) Imine based four-ring chalcone-ester liquid crystals: Synthesis, characterization, mesomorphic behavior and DFT approach. *Journal of Molecular Liquids*, **380**, 121719.

31. Mali, A. A. A., Jamain, Z. (2023) Synthesis and Characterization of Non-mesogenic behavior of chalcone derivatives. *Malaysian Journal of Chemistry*, **25**, 158–168.

32. Ahmed, H., Hagar, M., Saad, G. (2019) Impact of the proportionation of dialkoxy chain length on the mesophase behavior of Schiff base/ester liquid crystals; experimental and theoretical study. *Liquid Crystals*, **46**, 1611–1620.

33. Liu, J., Guan, L., Wang, Z. (2020) Phase behavior of surfactant mixtures and the effect of alkyl chain and temperature on lyotropic liquid crystal. *Colloids and Surfaces A: Physicochemical and Engineering Aspects*, **585**, 124019.

34. Segura, J. L., Mancheño, M. J., Zamora, F. (2016) Covalent organic frameworks based on Schiff-base chemistry: synthesis, properties and potential applications. *Chemical Society Reviews*, **45**, 5635–5671.

35. Jamain, Z., Khairuddean, M., Guan-Seng, T. (2020) Synthesis of novel liquid crystalline and fire retardant molecules based on six-armed cyclotriphosphazene core containing Schiff base and amide linking units. *RSC advances*, **10**, 28918–28934.

36. Dunmur, D. (2021) Liquid crystal chemistry and poetry. *Foundations of Chemistry*, **23**, 277–287.

37. Jamain, Z., Khairuddean, M., Guan-Seng, T., Rahman, A. B. A. (2021) Synthesis, characterization and mesophase transition of hexasubstituted cyclotriphosphazene molecules with Schiff base and azo linking units and determination of their fire retardant properties. *Macromolecular Research*, **29**, 331–341.

38. Lei, M., Sun, J., Chen, Y., Cai, Z., Hu, Y. (2022) The effect of alkyl chain length of the imidazole ionic liquid surfactants on the improving lubricating properties of the hexagonal lyotropic liquid crystal composed of the [C16imCn]Br/hydrotalcite/H2O. *Journal of Molecular Liquids*, **355**, 118918.

39. Ilincă, T. A., Chiriac, L. F., Ilis, M., Manaila-Maximean, D., Ganea, P. C., Pasuk, I., Cîrcu, V. (2022) Effect of disubstitution pattern of the terminal alkyl chains on the mesophase of liquid crystals based on lanthanide(III) complexes: A study of the thermal, emission and dielectric behavior. *Journal of Molecular Liquids*, **360**, 119425

40. Nagaveni, N. G., Roy, A., Prasad, V. (2012) Achiral bent-core azo compounds: Effect of different types of linkage groups and their direction of linking on liquid crystalline properties. *Journal of Material Chemistry*, **18**, 8948–8959

41. Jamain, Z., Khairuddean, M., Zulbaharen, N. N., Chung, T. K. (2019) Synthesis, characterization and determination of mesophase transition of azo-azomethine derivatives with different terminal chain lengths. *Malaysian Journal of Chemistry*, **21**, 73–85.

42. Heeley, E. L., Hughes, D. J., El Aziz, Y., Williamson, I., Taylor, P. G., Bassindale, A. R. (2013) Properties and self-assembled packing morphology of long alkyl-chained substituted polyhedral oligomeric silsesquioxanes (POSS) cages. *Physical Chemistry Chemical Physics*, **15**, 5518–5529.

43. Sharma, V. S., Patel, R. B. (2017) Effect of alkyl chain in the terminal ester group on mesomorphic properties of new rod like homologous series:

Synthesis and characterization. *Molecular Crystals and Liquid Crystals*, **643**, 62–75.

44. Andrienko, D. (2018) Introduction to liquid crystals. *Journal of Molecular Liquids*, **267**, 520–541.

45. Patel, R. B., Doshi, A. V. (2011) Synthesis and study of new ester homologous series: Ethyl-p-(p/-n/alkoxy cinnamoloxy)cinnamtes. *Der pharma Chemica*, **3**, 557–565.

46. Demus, D., Goodby, J., Gray, G. W., Spiess, H. -W., Vill, V. (1998) Handbook of Liquid Crystals. *Low Molecular Weight Liquid Crystals I; Wiley-VCH: New York, NY, USA*, **2A**.

47. Jamain, Z., Khairuddean, M., Saidin, S. A. (2019) Synthesis and characterization of 1, 4-phenylenediamine derivatives containing hydroxyl and cyclotriphosphazene as terminal group. *Journal of Molecular Structure*, **1186**, 293–302.

48. Mohammadya, S. Z., Al-Aasar, M., Fahmi, A. A. (2007) Possibility of mesophase formation in some model compounds based on the N-aryl benzamide group. *ThermochimicaActa*, **459**, 40–57.